Materials and Design 156 (2018) 528–537

Contents lists available at ScienceDirect

Materials and Design

journal homepage: www.elsevier.com/locate/matdes

Stretchable and magneto-sensitive strain sensor based on silver nanowire-polyurethane sponge enhanced magnetorheological elastomer

Tao Hu, Shouhu Xuan *, Li Ding, Xinglong Gong *

CAS Key Laboratory of Mechanical Behavior and Design of Materials, Department of Modern Mechanics, University of Science and Technology of China (USTC), Hefei 230027, PR China

HIGHLIGHTS

- The conductive magnetorheological elastomer (MRE) can be applied as tensile, compressive and magneto-sensitive sensor.
- The stiffness of matrix and filler content significantly influence the mechanic-electric properties of conductive MRE.
- The resistance of conductive MRE increases 91.8% and 67.6% under the tensile and compressive loading.
- The relative resistance increment of conductive MRE reaches as high as 100% under 428mT magnetic field.

GRAPHICAL ABSTRACT

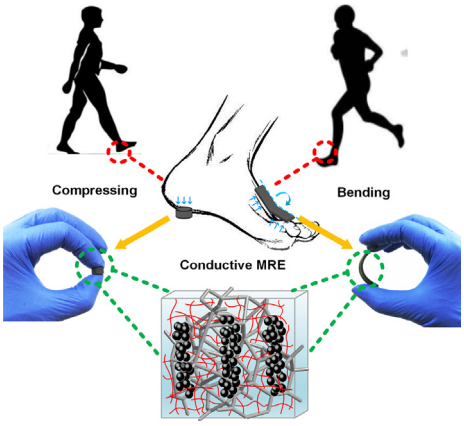

ARTICLE INFO

Article history:
Received 16 May 2018
Received in revised form 8 July 2018
Accepted 9 July 2018
Available online 20 July 2018

Keywords:
Magnetorheological elastomer
Polyurethane sponge
Strain sensor
Silver nanowire
Conductive

ABSTRACT

This work reported a stretchable, compressible and magneto-sensitive strain sensor based on conductive magnetorheological elastomer (MRE) containing silver nanowires (AgNWs) dip-coated polyurethane sponge, carbonyl iron particles and polydimethylsiloxane (PDMS) matrix. The mechanic-electric-magnetic coupling properties of conductive MRE were investigated and they were significantly influenced by mechanical properties of PDMS matrix and the AgNWs content. By increasing curing agent weight ratio, the cross-linking density of the PDMS increased thus the magneto-induced modulus decreased. The MRE was able to be used in the strain sensors, because its relative resistance variation reached 91.8% and 67.6% when 20% tensile strain and 10% compressive strain were applied. By applying a 428 mT magnetic field, the relative resistance of MRE sensor increased to 200%. Based on the experimental results, a possible mechanism was proposed to investigate the mechanic-electric-magnetic coupling sensing characteristics. Finally, the MRE sensors can be integrated on a shoe to detect the foot motion, demonstrated this material was promising in the intelligent devices like artificial skin, composite electrodes and soft sensor.

© 2018 Published by Elsevier Ltd.

1. Introduction

Due to the reversibly mechanical properties under magnetic field, magnetorheological elastomer (MRE) has attracted increasing

* Corresponding authors.
E-mail addresses: xuansh@ustc.edu.cn (S. Xuan), gongxl@ustc.edu.cn (X. Gong).

https://doi.org/10.1016/j.matdes.2018.07.024
0264-1275/© 2018 Published by Elsevier Ltd.

applications in vibration control [1], radio absorbing [2] and suspension system [3,4]. It was found that the natural frequency of MRE based devices could be significantly changed by applying magnetic field. Usually, MRE is mainly consisting of two parts: polymer matrix and magnetic particles. During the curing process, the constituents are mixed homogeneously in the presence of external magnetic field. Thus, the particles form linear structures aligned in the magnetic field direction in the final MRE. Over the past decades, numerous efforts have been conducted to improve mechanical properties of MRE [5–8]. Nevertheless, the traditional MREs were unsuitable for novel electrical devices like sensors due to the poor conductivity.

In order to meet the requirement of novel electrical devices, conductive fillers such as graphene, graphene oxide, graphite, and metal particles were incorporated into polymer matrix to improve the conductivity of magnetorheological (MR) materials. Pang et al. developed a novel MR material enhanced by graphite and the enhanced magnetic field dependent conductivity provided a new way for magnetic field detection [9]. Bica et al. fabricated a magnetoresistive sensor based on graphene enhanced MRE and discussed the influence of transverse applied magnetic field and compression pressure on the resistance to prove the potential towards a strain sensor [10]. The developments in portable and foldable electrical devices have heightened the need for stretchable and flexible sensors [11–15]. Sensors integrated with MR materials could synchronously reflect the strength of stimulation applied to the devices by identifying the varied mechanical state of component, which was very important in practical application. So flexible and conductive sensors based on MR materials were fabricated.

The responsive of sensors under external stimulation like stretching and compressing is mostly dependent on the variation of electrical properties such as resistance or capacitance. Both sensitivity and stretchability should be taken into consideration to manufacture high performance sensors. To supersede the traditional rigid sensors, several stretchable and flexible sensors, for example, conductive additives deposited on flexible substrates [16–22], conductive networks or films [23–27] and other alternative fillers like conductive foams or sponges embedded in different substrates were manufactured [28–34]. Very recently, three dimensional (3D) structures enhanced flexible sensors have attracted great interests due to excellent conductivity and stretchability. After incorporating these 3D conductive structures into the elastomeric substrate such as polydimethylsiloxane (PDMS), flexible hybrids with interconnected conductive networks were achieved. Jun et al. prepared conductive graphene-PDMS composite by infiltrating 3D reduced graphene oxide foams with PDMS and it was found large graphene could significantly enhance conductivity of composite [35]. Ge et al. fabricated elastomeric and magnetic strain sensors with high conductivity and stretchability by incorporating the conductive carbon nanotubes coated polyurethane sponge (PUS) into MRE, the PUS/MRE was demonstrated to be applied as strain sensors due to the strengthening 3D topological scaffold and the stable strain dependent resistance [36]. However, these sensors would suffer from weak stretchability, low gauge factor and large hysteresis due to the brittleness and weak adhesion of conductive materials.

Because of the excellent electrical, mechanical and optical properties, silver nanowires (AgNWs) have attracted great attention for the potential application in sensors [37–43]. Amjadi et al. reported a sandwich-structured strain sensor with high stretchability based on AgNW-PDMS composite which could be integrated into a glove to detect finger motion [44]. Ge et al. fabricated a stretchable conductor based on PUS-AgNW-PDMS composite with novel interconnected binary networks, the excellent conductivity and stability enabled itself to be used for future electric devices [45]. So traditional MRE could be markedly enhanced by AgNW based 3D conductive structures and the final product will attract much attention in novel electric devices due to their excellent mechanical and electrical properties.

The previous work [36] mainly focused on the rheological properties and tensile sensing performance of MRE featuring carbon nanotubes dip-coated PUS. Meanwhile, this paper emphasized the enhancement of filler material content and curing agent ratio on rheological behaviors, and the potential of MRE as a multifunctional strain sensor. Not only tensile, but also compressive and magnetic sensing performance were investigated to understand the magnetic-mechanic-electric coupling behavior. In this paper, AgNW/PUS was immersed into carbonyl iron particles (CIPs) doped PDMS matrix to develop a novel conductive MRE. Strain sensors based on conductive MRE showed good electrical and mechanical properties because of the 3D interconnected AgNW networks coated PUS backbones and CIPs chain-like structures. The responsive of sensors under cyclic tensile, compressive and magnetic loading was investigated. Possible sensing mechanisms were proposed to discuss the influence factors on the sensing performance. Finally, a shoe integrated with MRE sensors was developed for the motion detection of foot.

2. Experimental section

2.1. Materials

The PDMS (type Sylgard 184) precursor and curing agent were purchased from Dow Corning GmbH, USA. CIPs (type CN) with an average diameter of 6 μm from BASF were used as magnetic particles. Polyvinylpyrrolidone (PVP), $AgNO_3$, glycerol, ethanol and NaCl were from Sinopharm Chemical Reagent Co., Ltd. Deionized water was self-prepared. Commercially available PUSs were used as the 3D scaffold.

2.2. Preparation

Silver nanowires (AgNWs): 5.86 g PVP was added into 190 mL glycerol, then the mixture was heated to 90 °C and cooled to 50 °C under stirring (~100 rpm) to make PVP fully dissolved. Afterward, 1.58 g $AgNO_3$ and a solution containing 58 mg NaCl, 0.5 mL deionized water and 10 mL glycerol were added and heated up to 210 °C in 20 min under slow stirring (~50 rpm). Ultimately, the heater was moved away and the gray-green solution in flask was transferred to a beaker. After a week's stably stratification, a layer of sediment containing AgNWs at the bottom of beaker was collected. The obtained AgNWs were washed by deionized water, then the solution was centrifuged under 7000 rpm for 15 min, the upper layer of solution was poured out and the sediment was washed again.

Conductive PUSs: Porous PUSs were cut into small pieces with the dimension of 20 mm in diameter and 1 mm in thickness for rheological tests, 2 mm in thickness and width by length of 10×50 mm^2 for tensile tests and 10 mm in diameter and 5 mm in thickness for compressive tests. The pieces were all cleaned by deionized water twice, immersed in acetone for 2 h, and dried at 80 °C for 2 h. Then, the pieces were immersed into the ethanol solution of AgNWs (~1.5 mg/mL), moved into oven, and dried at 80°C for 4 h. By repeating the dip-coating procedure for 3, 4, 5 and 6 times, PUSs with different conductivity (marked as 3rd, 4th, 5th and 6th dip-coated conveniently) were obtained. Copper wires were adhered to both the ends of conductive PUSs for tensile tests longitudinally, as well as the top and bottom of conductive PUSs for compressive tests by silver conductive paint to test the electrical properties (Fig. 1).

Conductive MREs: At first, magnetorheological (MR) precursor with different curing agent weight ratio (1:10, 1:20, 1:25 and 1:30) of PDMS matrix was prepared. The CIPs, PDMS matrix and curing agent were mixed in a beaker for 10 min. Then the beaker was transferred into ultrasonic machine which was kept at 80% power for 10 min to further separate. The weight fraction of CIPs was 60 wt% for all MR precursor. Conductive PUS pieces were immersed into MR precursor, then transferred into a vacuum oven and treated for

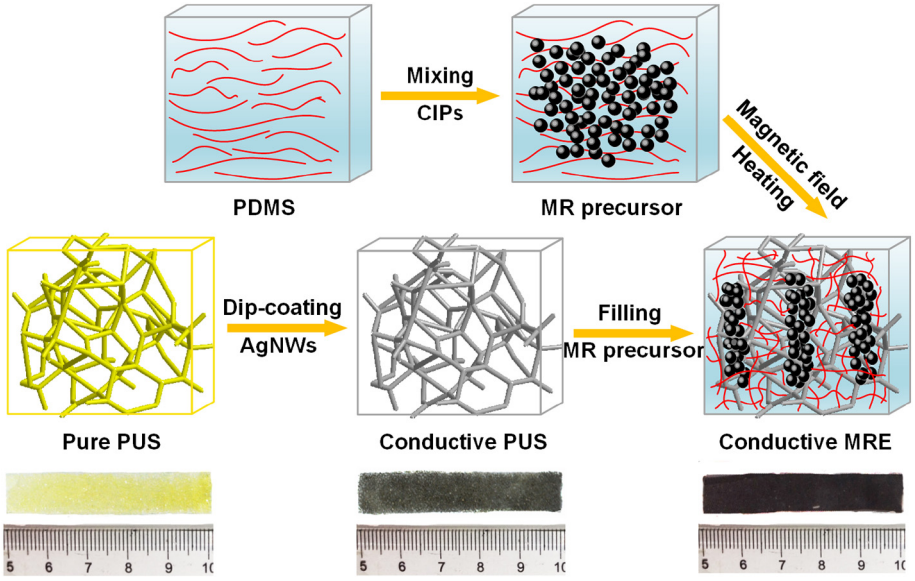

Fig. 1. Fabrication processes and photographs of the conductive MRE.

20 min to ensure the porous structures of conductive PUS were fully filled. The pieces were put into molds and followed by thermally curing for 10 min at 50°C and 15 min at 110°C under 1 T magnetic field. Magnetic field was applied perpendicularly to the surface of MREs to form chain-like structures of CIPs. For convenience, different conductive MREs were defined as X-Y MRE, where X was the dip-coating cycles of PUS and Y was curing agent weight ratio of PDMS matrix.

2.3. Characterization

The morphology of conductive PUSs and MREs were observed by an environment scanning electron microscope (SEM, Philips of Holland, model XL30 ESEM-TMP) under 15 kV.

The rheological properties of conductive MREs were measured by a commercial rheometer (Physica MCR 301, Anton Paar Co., Austria). The cylindrical samples were placed between the parallel plate and electromagnet. By applying 0 to 4 A current, 0 to 1000 mT magnetic field was generated perpendicularly to the surface of samples. The rheometer worked under shear oscillation mode during tests, the shear frequency was set at 10 Hz and the shear amplitude varied from 0.1%, 0.3% to 0.5%. The temperature of testing system was controlled at 25°C.

A universal testing machine (MTS criterion 43, MTS System Co., America) was employed for cyclic tensile and compressive tests. The force and displacement were collected and analyzed by computer to study the mechanical properties. The strain amplitude changed from 20%, 30% to 40% and the strain rate was 50 mm/min, 100 mm/min, 150 mm/min, 200 mm/min and 250 mm/min. Both ends of sensor were fixed with the clamps, about 10×10 mm^2, thus the stretchable area of sensor was 10×30 mm^2. As for compressive tests, two electromagnet coils were fixed with the clamps and a programmable power was attached to the coils. The coils could generate 0 to 428 mT magnetic field by applying 0 to 1.25 A current. The strain amplitude changed from 6%, 8% to 10% and the strain rate was 2 mm/min, 4 mm/min and 8 mm/min. The compressive strain sensors were placed centrally between the coils and the magnetic field was applied perpendicularly to the surface of samples.

When sensors were subjected to tensile or compressive loading, Modulab® material test system (Solartron analytical, AMETEK advanced measurement technology, Inc., United Kingdom) was employed to test the electrical properties at the same time. Direct current voltage excitation was supplied to the samples and the responsive of current was measured. The output voltage was set at 4 V and copper wires were connected to Modulab by two signal lines. A Tesla meter (HT20, Shanghai Hengtong magnetic technology Co. Ltd, China) was used to measure the magnetic flux density in the gap between two coils.

3. Results and discussions

3.1. Microstructure of conductive PUSs and MREs

The SEM images showed that both of the pure PUS and Ag/PUS (Fig. 2a–b) exhibited the cellular-like porous structure. After dip-coating the AgNWs, many white area randomly distributed on the backbones of conductive PUS, indicated that AgNWs were successfully immobilized (Fig. 2c). The AgNWs contacted with each other and the conductive paths were formed. The incorporation of PDMS/CI hybrid into the cellular pores could further stabilize the conductive network. As shown in Fig. 2d, the PDMS was tightly adhered on the surface of PUS backbones. Here, the AgNWs were firmly sandwiched between PDMS and PUS, which enable them to be applied in resistive sensors.

The PDMS/CI precursor was cross-linked within the PUS sponge under the magnetic field, thus the CIPs formed chain-like structures in matrix and they were assembled along the direction of applied magnetic field (Fig. 2e–h). Undoubtedly, with increasing of curing agent weight ratio (PDMS), the chain-like structures decreased, and the combination among CIPs and PDMS matrix was weakened (Fig. SI 1). The cross-link density of PDMS matrix gradually increased with curing agent content, which resulted in stronger binding force, thus the movement of molecular chains significantly reduced. As a result, mechanic-electric-magnetic coupling properties of conductive MREs extremely depended on curing agent weight ratio of PDMS matrix.

3.2. Rheological properties of conductive MREs

In this work, the rheological properties of MR precursor (consisting of liquid PDMS and magnetic CI particles) was tested, the shear rate was 10 s^{-1} and the temperature was 30 °C (Fig. 3a). With increasing of curing agent ratio, the viscosity changed from 7.49 Pa·s to 5.02 Pa·s and it was relatively stable during the test. By increasing the temperature, the viscosity of MR precursor also changed little (Fig. 3b). When the PUS were fully immersed in MR precursor and treated in vacuum

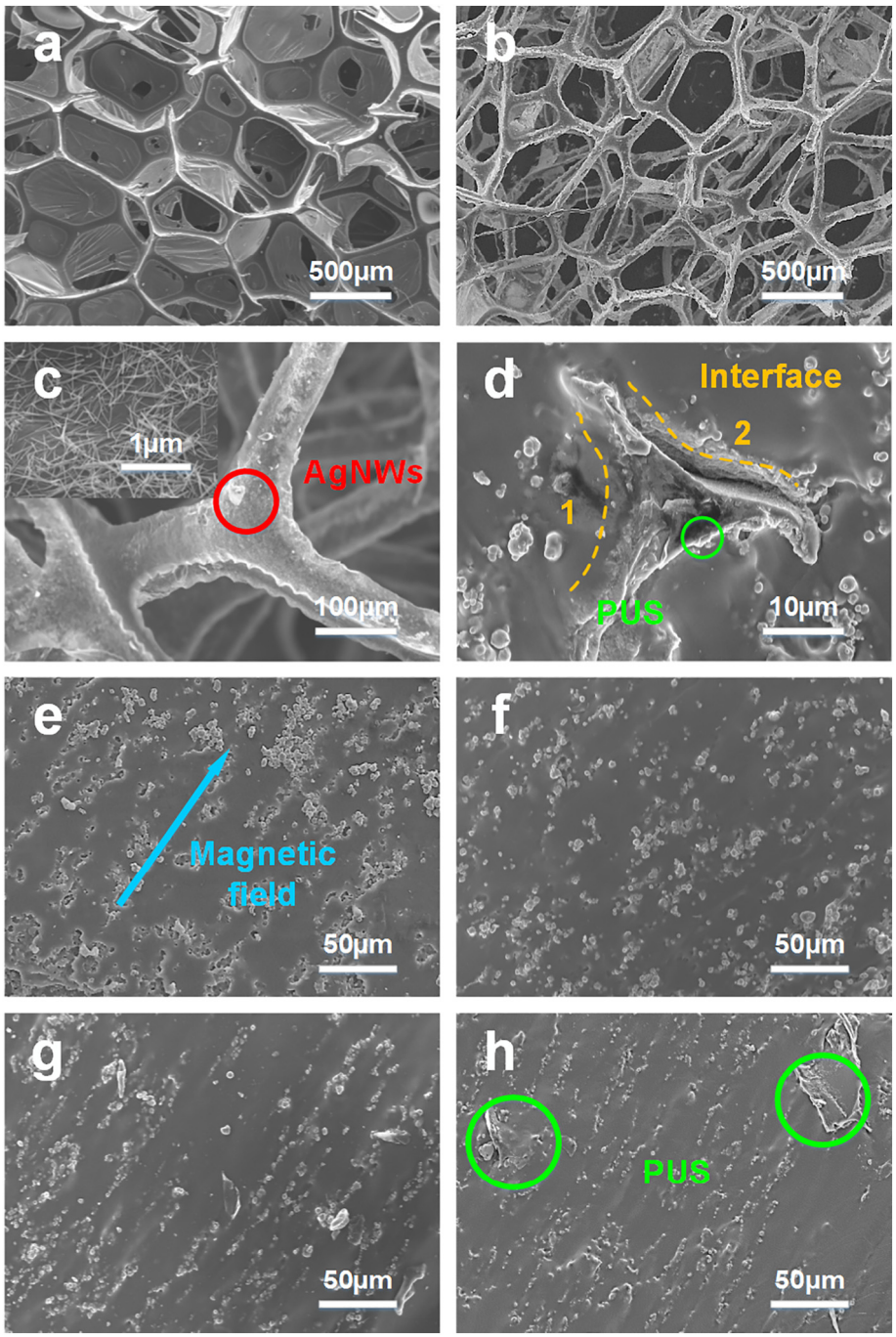

Fig. 2. SEM images of (a) pure PUS; (b)–(c) conductive PUS; (d) PUS backbones immersed in PDMS matrix; (e)–(f) conductive MREs with 1:10, 1:20, 1:25 and 1:30 matrix.

oven, the Ag/PUS percolation networks should be penetrated by liquid PDMS.

The conductive MREs with different dip-coating cycles and curing agent weight ratio were prepared. The curing agent weight ratio of PDMS matrix was set at 1:20, testing frequency and amplitude was 10 Hz and 0.3%. With increasing magnetic field from 0 to 1000 mT, the storage modulus gradually increased for all samples, it changed from 0.19 MPa to 0.38 MPa for MRE with 5th dip-coated PUS (Fig. 3c). Here magnetorheological (MR) effect was defined as $G_m/G_0 = (G_s - G_0)/G_0$ in which G_m was magnetic-induced modulus, G_0 was initial modulus and G_s was largest storage modulus during the test. Clearly, with increasing of dip-coating cycles, the G_0 gradually decreased as well as G_s, which indicated the decrease of mechanical performance. Both of the G_0 and G_s for samples without PUS were lower than PUS incorporated samples, demonstrated the enhancement of PUS. Moreover, it could be seen the loss factor gradually decreased with increasing of dip-coating cycles and magnetic field (Fig. 3d). The content of AgNWs on PUS backbones increased with increasing of dip-coating cycles, which further enhanced the 3D conductive structures. However, the movement of PDMS molecular chains was reduced and the energy dissipation gradually decreased. As a result, the mechanical performance was weakened with increasing of dip-coating cycles.

Moreover, the effect of curing agent weight ratio on the rheological properties of the conductive MRE was investigated. With increasing magnetic field from 0 to 1000 mT, the storage modulus significantly increased. Keeping curing agent weight ratio of 1:30, it ranged from

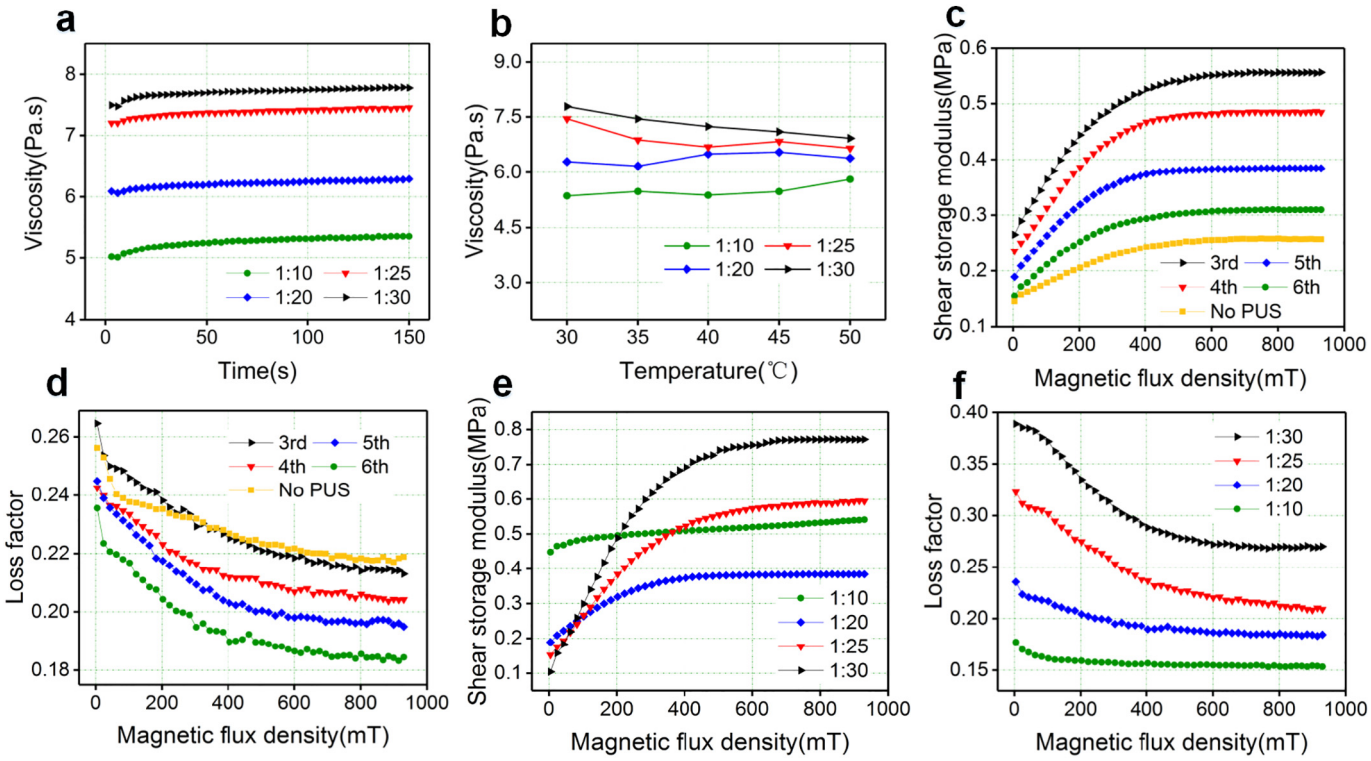

Fig. 3. The rheological properties of (a)–(b) MR precursor and conductive MREs with (c)–(d) different dip-coating cycles; (e)–(f) different curing agent weight ratio.

0.10 MPa to 0.77 MPa (Fig. 3e). With increasing of curing agent weight ratio, the G_0 increased, but the MR effect significantly reduced (from 660% to 20%), which indicated the decrease of magnetic-induced performance. Then, the loss factor decreased with increasing of curing agent content (Fig. 3f). The loss factor also showed a downtrend under the increased magnetic field. With increasing of curing agent weight ratio, the cross-link density of PDMS matrix increased, which led binding force to be stronger. Therefore, the movement of PDMS molecular chains was reduced, the energy dissipation and chain-like structures' number decreased, which agreed with the SEM images of conductive MREs. So both the damping and magnetic-induced performance were weakened with increasing of curing agent weight ratio.

To further study the rheological properties of different samples, the G_m under different testing amplitude (0.1%, 0.3% and 0.5%) was obtained (Fig. SI 2). Under the same testing amplitude, the G_m decreased with increasing of dip-coating cycles and curing agent weight ratio. Consequently, samples with 1:30 matrix showed excellent magnetic-induced performance but extremely low strength while samples with 1:10 matrix were stiff but showed weak magnetic-induced performance. So 1:20 was selected as the ideal curing agent weight ratio due to the suitable strength and good magnetic-induced performance.

3.3. Tensile strain responsive performance of conductive MRE sensors

The electrical properties of conductive MREs relied on the AgNW networks and molecular chains in PDMS matrix. Under the tensile and compressive strain, the AgNW networks deformed under the external applied stimulation. Here, the electromechanical properties of the conductive MREs were studied and the responsive of conductive MRE sensors under cyclic tensile loading was tested.

The conductive MRE sensors with different curing agent weight ratio and dip-coating cycles were tested by increasing the tensile strain from 0 to 20% at 100 min/mm. Here the relative resistance variation was defined as $\Delta R/R_0 = (R - R_0)/R_0$ in which R_0 was the initial resistance, R was the resistance during testing and ΔR was resistance variation. The responsive of 5th dip-coated conductive MRE sensors with different curing agent weight ratio in stretch and release cycles was tested (Fig. 4b). With increasing of tensile strain from 0 to 20%, the R of conductive MRE sensors with curing agent weight ratio of 1:20 synchronously increased from to 0.27 kΩ to 0.32 kΩ. The $\Delta R/R_0$ of different sensors showed good linear relationship with increased tensile strain and the tensile sensing performance was compared with the previous results in reference [44] (Fig. 4c). With increasing of curing agent weight ratio, both the ΔR and R_0 significantly decreased, thus reduced the sensing performance. It was observed the tensile stress of different sensors could return to original state after several cycles, which represented excellent elasticity and resilience (Fig. 4d).

A mechanism was proposed to investigate the influence of curing agent weight ratio on sensing performance (Fig. 5). With increasing of curing agent weight ratio, the increased crosslinks reduced the number of free PDMS molecular chains. Then the contact area among free PDMS molecular chains and AgNW networks also reduced, so the interaction of AgNWs and PDMS molecular chains decreased. More conductive paths formed by AgNW networks could be remained, which resulted in the decrease of ΔR and R_0. The tensile failure tests of samples with different curing agent ratio were conducted to compare the tensile strength (Fig. SI 3). All the samples represented elastic deformation and destruction stages. With increasing of curing agent weight ratio, more PDMS molecular chains were entangled and interacted due to the increased cross-links inside matrix, so the tensile strength of samples was improved.

Moreover, the effect of dip-coating cycles on electrical properties was investigated (Fig. 4e). The more dip-coating cycles of PUS, the higher conductivity. With increasing of dip-coating cycles, the mass content of AgNWs on the PUS backbones increased. Then, the contact area among AgNWs also increased and more effective conductive paths were formed, which further improved the conductivity. The 3th dip-coated samples showed good mechanical performance but poor conductivity, while 6th dip-coated samples obtained good conductivity but weakened mechanical performance. So 5th dip-coated PUS was

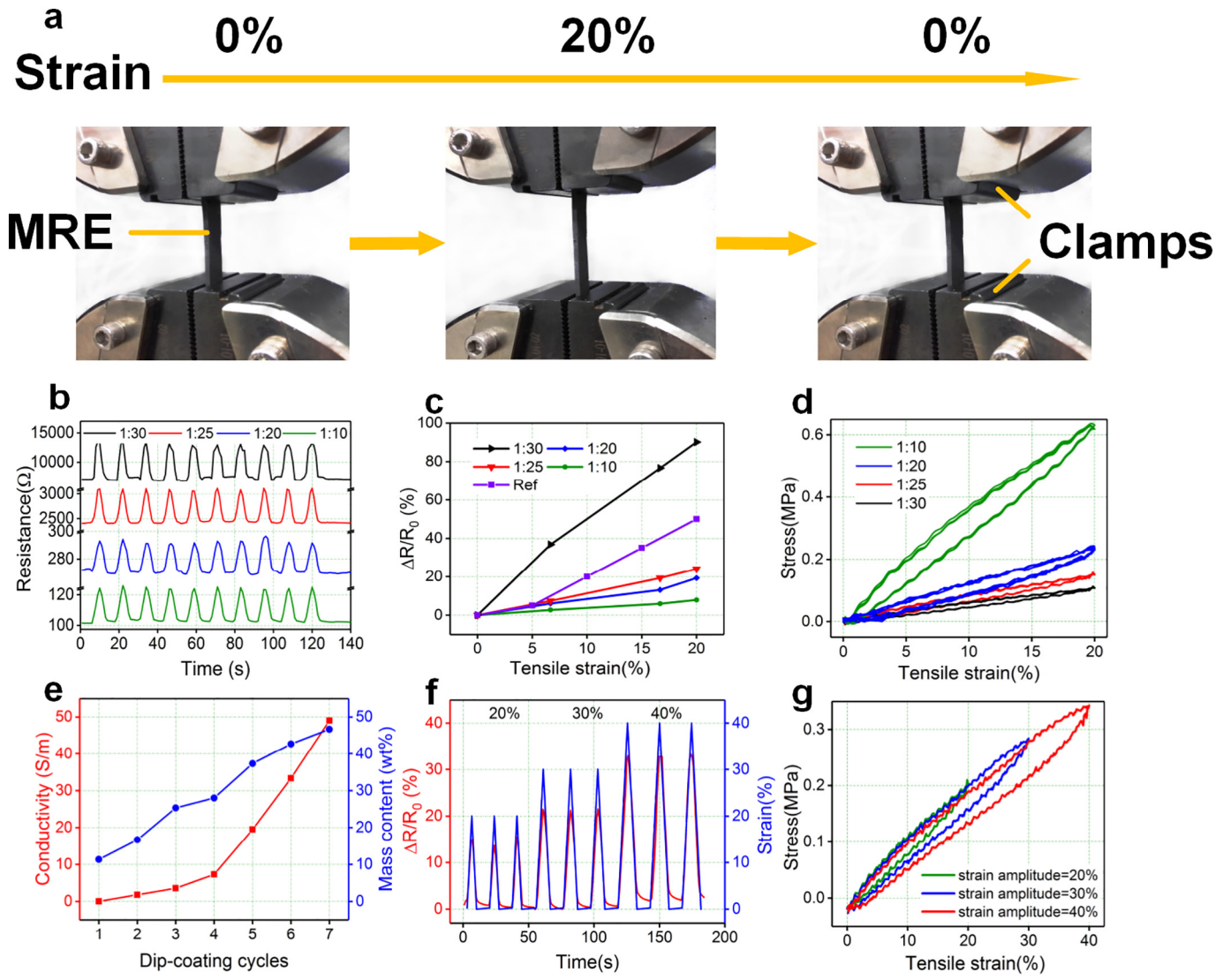

Fig. 4. (a) The tensile testing system: clamps of universal testing machine and sensor; (b)–(d) resistance, relative resistance and tensile stress variation for sensors with different curing agent weight ratio under cyclic tensile loading; (e) conductivity and mass content of conductive PUS with different dip-coating cycles; (f)–(g) relative resistance and tensile stress variation of 5th-1:20 MRE sensor under cyclic tensile loading with different tensile strain amplitude.

selected due to the good conductivity and ideal strength. After being fully immersed in PDMS/CI precursor, the 3D conductive structures of Ag/PUS were maintained, then the final MREs processed high conductivity.

Because of the suitable tensile strength and stable sensing performance, the 5th-1:20 MRE sensor was selected to test the electrical properties under different tensile strain amplitude at 100 mm/min (Fig. 4f). The $\Delta R/R_0$ gradually increased with increasing tensile strain from 20% to 40%. It reached 33% under 40% tensile strain, and returned to original state in each stretch-release cycle. The tensile stress was measured synchronously and the variation tendency was similar progress under different strain amplitude. In addition, the tensile rate showed few effect on the ΔR of conductive MRE sensor (Fig. SI 4), which further demonstrated the conductive MRE was stable enough for as a tensile strain sensor.

3.4. Compressive strain responsive performance of conductive MRE sensors

It was necessary to explore the compressive strain responsive of conductive MRE sensors since MREs were often used under compression or vibration. Keeping the compressive rate and strain amplitude as 4 mm/min and 10% respectively, the compressing electromechanical properties of the MRE were tested by universal testing machine. The R increased with compressive strain (0 to 10%) and it ranged from 28.7 Ω to 31.8 Ω for 1:20 matrix MRE sensors (Fig. 6a). The $\Delta R/R_0$ linearly increased with compressive strain and the compressive sensing performance was compared with the previous results in reference [33] (Fig. 6b). With increasing of curing agent weight ratio, both the ΔR and R_0 significantly decreased, which agreed with the results in Fig. 4c. At the same time, the compressive stress variation of samples with different curing agent weight ratio was recorded. The compressive stress reached 0.41 MPa for samples with 1:20 matrix under compressive strain of 10% (Fig. 6c), which indicated that the PDMS matrix was strengthened by curing agent. With increasing of curing agent weight ratio, more cross-link points were formed inside the PDMS matrix and the movement of molecular chains was reduced, resulted in a large increase of compressive stress (434%). A mechanism was proposed to describe the sensing performance of conductive MRE sensors under compressive strain (Fig. 7). When compressive strain was applied, it could be shared by PUS backbones. Then the AgNW percolation networks on PUS backbones deformed and they would detach from each other, thus resistance increased.

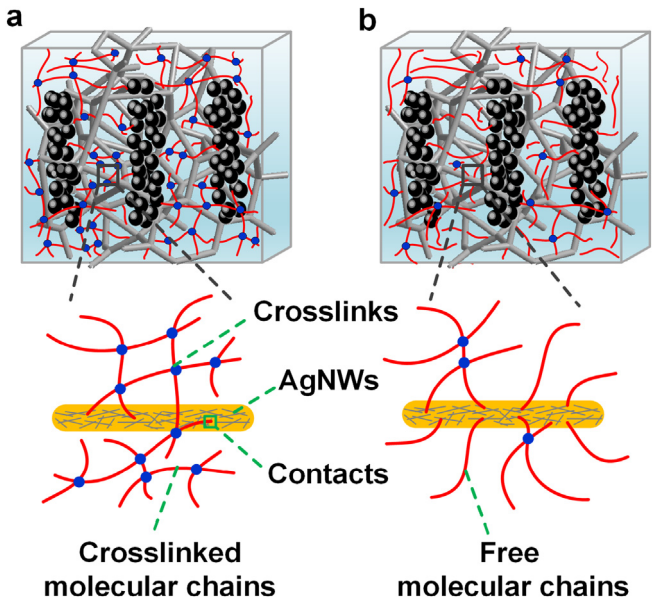

Fig. 5. Schematic illustrations for the sensing mechanism of conductive MRE sensors with (a) high curing agent weight ratio; (b) low curing agent weight ratio.

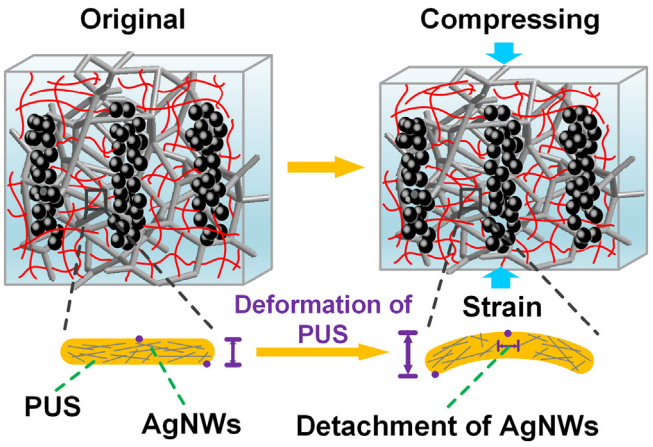

Fig. 7. Schematic illustrations for the sensing mechanism of conductive MRE sensors under compressive strain.

The 5th-1:20 MRE sensor possessed good compressive strength and stable sensing performance. The cycle ΔR under different compressive rate (2 mm/min, 4 mm/min and 8 mm/min) was kept almost as a constant (Fig. 6d), which proved the conductive MRE was proper for a compressive strain sensor. The $\Delta R/R_0$ and compressive stress under different compressive strain amplitude was also tested (Fig. 6e–f). With increasing the compressive strain from 6% to 10%, the $\Delta R/R_0$ increased and it reached 11.1% under 10% compressive strain. The variation tendency of compressive stress was similar in each cycle, and the hysteresis loops demonstrated a typical viscoelasticity of MRE (Fig. 6f). The upper parts of hysteresis loops under different compressive strain amplitude were overlapped, which proved good mechanical stability of conductive MREs.

3.5. Magnetic responsive performance of conductive MRE sensors

The MREs exhibited excellent magnetic field dependent conductivity. For the MRE based on the 5th dip-coated PUS, the R of conductive MRE sensors significantly increased with magnetic field. By applying a 428 mT magnetic field, it varied from 28.1 Ω to 29.8 Ω (Fig. 8b). With increasing of dip-coating cycles, the content of AgNWs on PUS backbones gradually increased, which decreased the $\Delta R/R_0$ from 100% to 4.5%. Fig. 9 showed the schematic mechanism of the magnetic sensing performance. Due to the magnetic interaction of CIP chains, the reactive

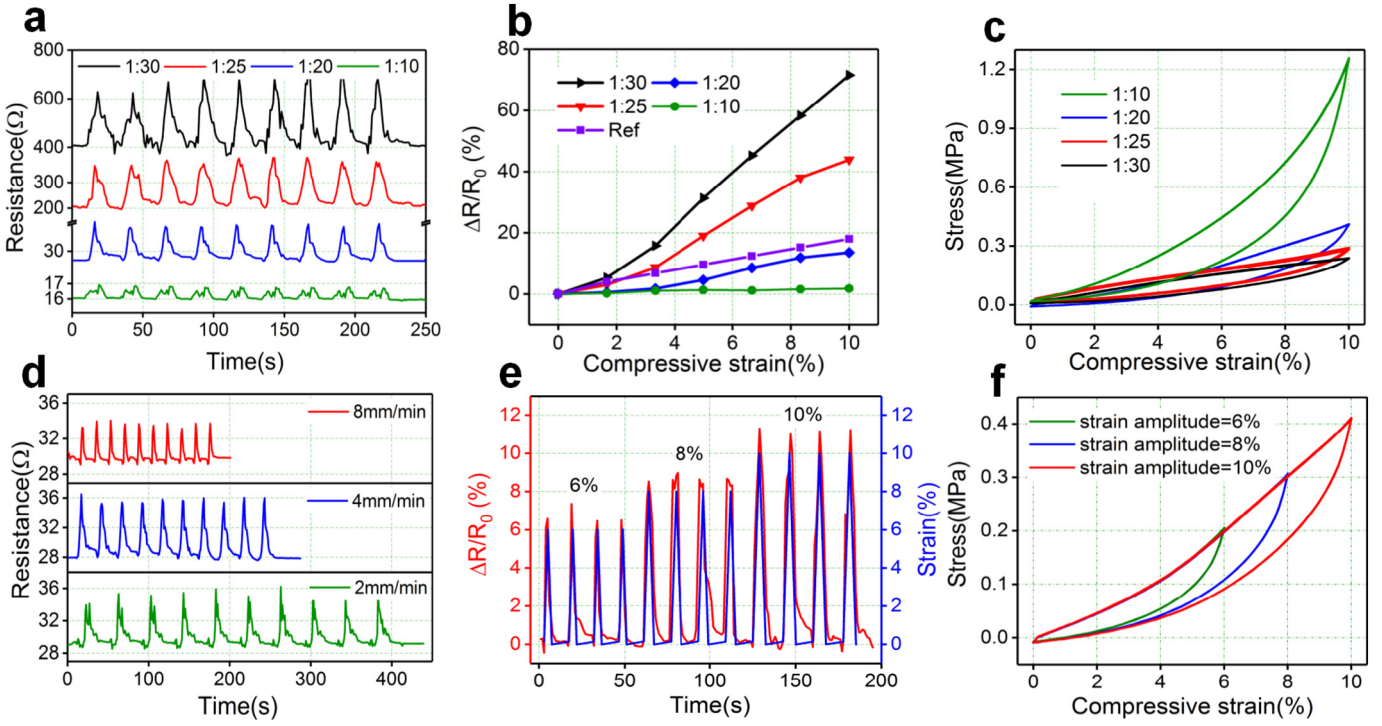

Fig. 6. (a)–(c) Resistance, relative resistance and compressive stress variation of sensors with different curing agent weight ratio under cyclic compressive loading; (d) the resistance variation of 5th-1:20 MRE sensor under different compressive strain rate; (e)–(f) relative resistance and compressive stress variation of 5th-1:20 MRE sensor under different compressive strain amplitude.

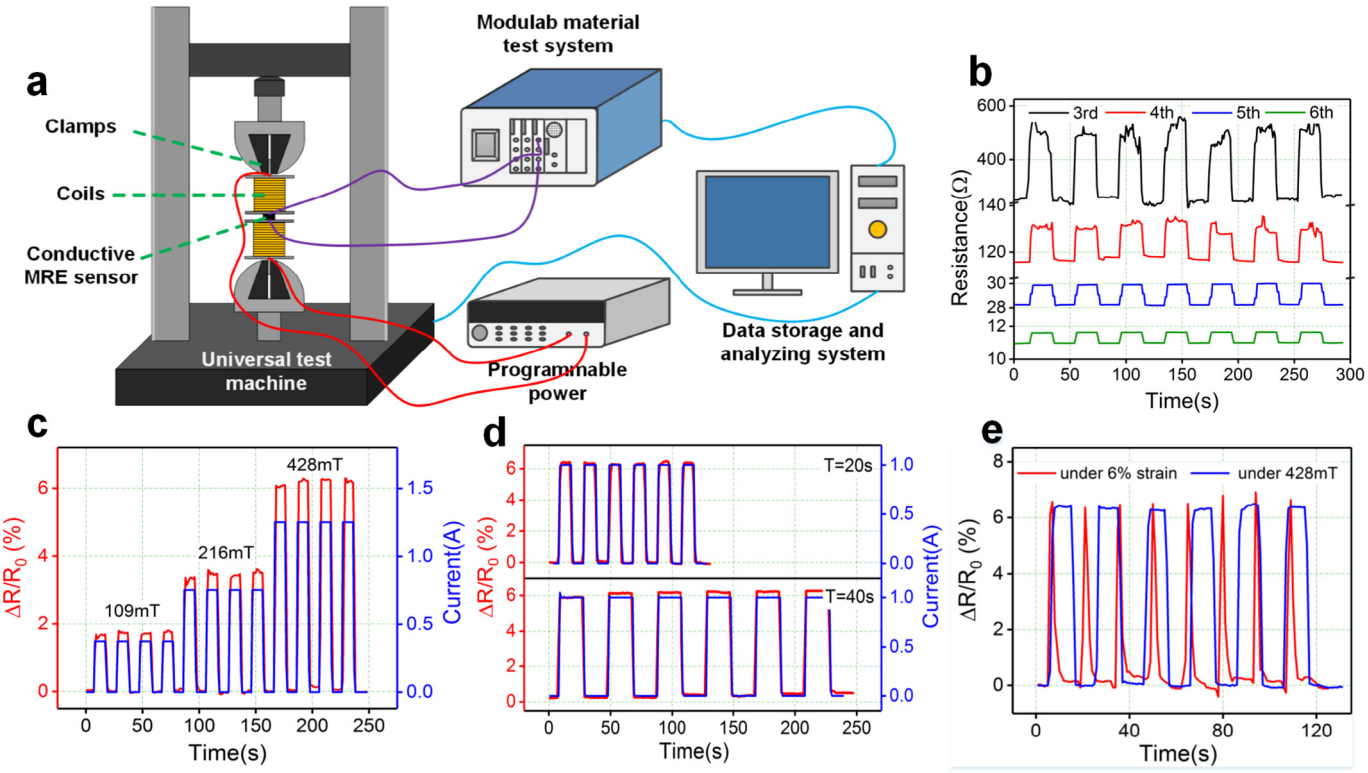

Fig. 8. (a) Schematic illustrations for the compressive and magnetic testing system; (b) the resistance variation of sensors with different dip-coating cycles under cyclic magnetic field; (c)–(d) the relative resistance variation of 5th-1:20 MRE sensor under different magnetic flux density and cycle length; (e) the comparison between compressive strain and magnetic responsive of 5th-1:20 MRE sensor.

force between PDMS molecular chains and CIP chains increased with the magnetic field. In this case, both the PDMS matrix and PUS backbones deformed, the contact area of AgNWs on PUS backbones were broken and restructured, thus the electrical properties varied.

Fig. 8c showed the cycling magnetic responsive of 5th-1:20 MRE sensor under different magnetic flux density and cycle length. When magnetic field was changed from 109 mT to 428 mT, the $\Delta R/R_0$ increased. Then the $\Delta R/R_0$ under different cycle length (20 s and 40 s) was tested (Fig. 8d). Clearly, the magnetic flux density and cycle length hardly affected the sensitivity, which proved the stability of conductive MRE. Finally, it was very interesting to find that the $\Delta R/R_0$ obtained by 6% compressive strain was similar to the one achieved by 428 mT magnetic field (Fig. 8e). This result indicated that both the strain and magnetic field could synergistically affect the sensing activity of the conductive MRE sensor. Here, the mechanic-electric-magnetic coupling properties of the MRE sensor are very complicated and more work will be done to clear the detail mechanism.

3.6. Application of conductive MRE sensors

Due to the good tensile, compressive and magnetic sensing performance, the conductive MREs could be applied as a strain sensor. In

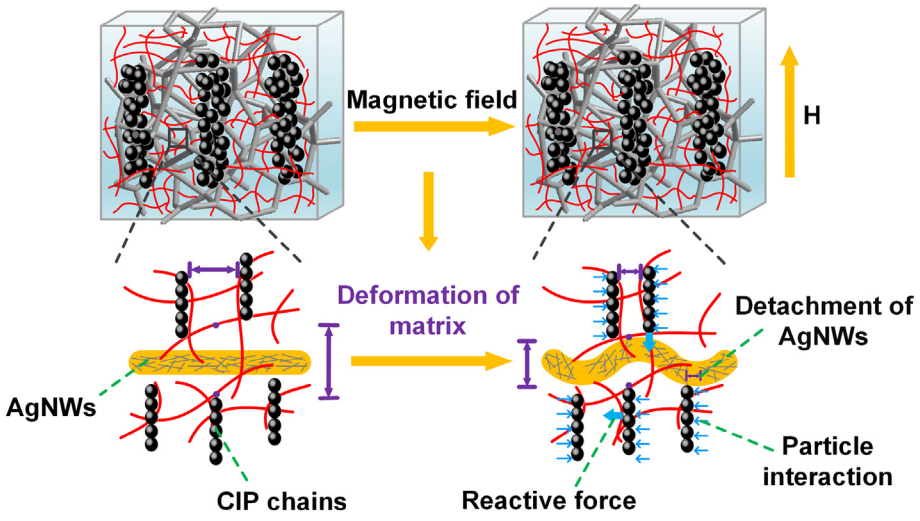

Fig. 9. Schematic illustrations for the sensing mechanism of conductive MRE sensors under applied magnetic field.

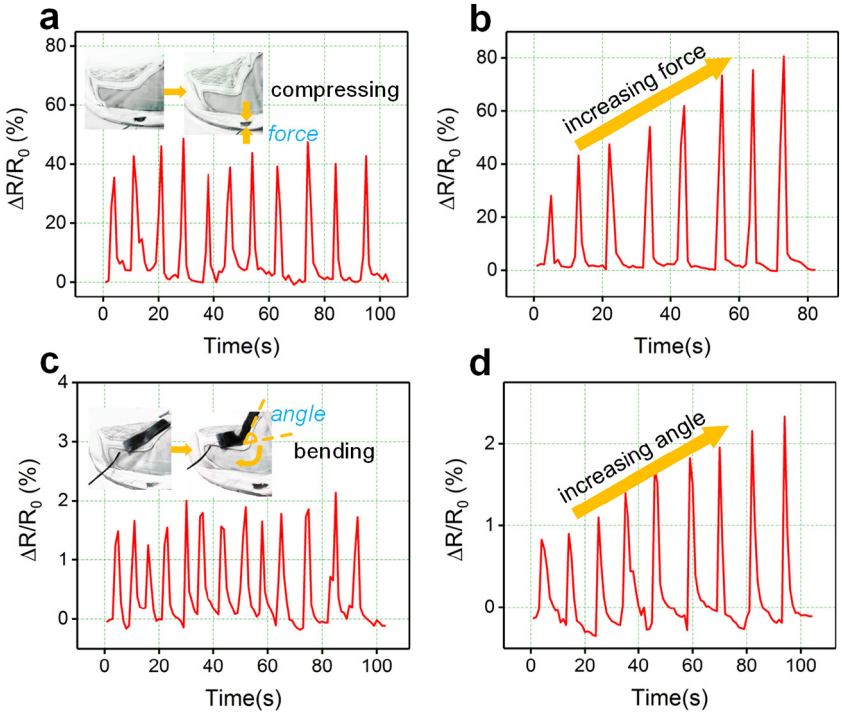

Fig. 10. Time-dependent relative resistance variation of conductive MRE sensors to detect human walking: (a)–(b) compressive strain sensor attached to the middle of sole; (c)–(d) tensile strain sensor attached to the vamp.

this work, the conductive MRE sensor was used to detect the human motion. The 5th-1:20 MRE compressive and tensile strain sensor were integrated on a human shoe and the response of sensor was tested. The compressive strain sensor was put into the middle of front sole to detect the compression force of forefoot. During the human walking, the forefoot firstly contacted with the top of fore sole and the bottom touched with the ground, then the front sole was compressed by the tighten muscles and the reactive force of ground supported the continued motion of human. The $\Delta R/R_0$ increased to 35.4% with the applied compressive force, its response was stable under similar walking speed (Fig. 10a). With increasing of walking speed, the human body was accelerated, so the foot pressure on the sensor also increased, which resulted in the significant increase of the $\Delta R/R_0$ from 27.9% to 80.5% (Fig. 10b).

After the forefoot contacted the sole, this foot was bent to raise the heel and supported the motion of body. The tensile strain sensor was attached to the vamp above forefoot to detect the bending of foot. The $\Delta R/R_0$ increased to 1.9% as the foot was bent, it could be kept under similar walking speed (Fig. 10c). With increasing of walking speed, larger bending angle of forefoot was required to accelerate the human body, thus the $\Delta R/R_0$ increased from 0.8% to 2.3% (Fig. 10d). During the whole motion detection, there was no considerable drifting or hysteresis between the dynamic loading and the responsive of the sensors. Hence, the conductive MRE sensors could serve as the accurate motion detection due to the good mechanical and electrical stability.

4. Conclusion

In summary, a novel conductive MRE consisting of PDMS, PUS, AgNWs and CIPs were developed. The AgNWs were dip-coated on PUS backbones to form interconnected networks and CIPs formed chain-like structures during the further fabrication of conductive MRE. The strain sensors based on conductive MREs were demonstrated to have good sensitivity under cyclic tensile and compressive loading. With increasing of curing agent weight ratio and dip-coating cycles, the magnetic-induced and sensing performance of conductive MREs were weakened. Moreover, the response of sensors could be synchronously controlled by the applied magnetic field, which indicated conductive MREs could also serve as magnetic sensor. Hence, the good mechanical strength and sensing performance make conductive MREs become prospective material for future employment in flexible, stretchable and conductive sensor devices.

Author contributions section

Tao Hu performed all the experiments and wrote the draft of the manuscript. Tao Hu, Shouhu Xuan, Li Ding and Xinglong Gong revised and discussed the manuscript.

Acknowledgement

Financial supports from the National Natural Science Foundation of China (Grant Nos. 11572310, 11572309) and the Strategic Priority Research Program of the Chinese Academy of Sciences (Grant No. XDB22040502) are gratefully acknowledged. This work is also supported by the Collaborative Innovation Center of Suzhou Nano Science and Technology, National Synchrotron Radiation Laboratory, USTC (KY2090000031).

Data availability

The authors declare that the data supporting this study are available within the article. Furthermore, extra data are also available from the corresponding author upon request.

Appendix A. Supplementary data

Supplementary data to this article can be found online at https://doi.org/10.1016/j.matdes.2018.07.024.

References

[1] G. Liao, Y. Xu, F. Wei, R. Ge, Q. Wan, Investigation on the phase-based fuzzy logic controller for magnetorheological elastomer vibration absorber, J. Intell. Mater. Syst. Struct. 28 (6) (2017) 728–739.

[2] M. Cvek, R. Moucka, M. Sedlacik, V. Babayan, V. Pavlinek, Enhancement of radio-absorbing properties and thermal conductivity of polysiloxane-based magnetorheological elastomers by the alignment of filler particles, Smart Mater. Struct. 26 (9) (2017), 095005.

[3] S.S. Sun, D.H. Ning, J. Yang, H. Du, S.W. Zhang, W.H. Li, A seat suspension with a rotary magnetorheological damper for heavy duty vehicles, Smart Mater. Struct. 25 (10) (2016) 105032.

[4] S.B. Choi, W.H. Li, M. Yu, H.P. Du, J. Fu, P.X. Do, State of the art of control schemes for smart systems featuring magneto-rheological materials, Smart Mater. Struct. 25 (4) (2016), 043001.

[5] J.S. An, S.H. Kwon, H.J. Choi, J.H. Jung, Y.G. Kim, Modified silane-coated carbonyl iron/natural rubber composite elastomer and its magnetorheological performance, Compos. Struct. 160 (2017) 1020–1026.

[6] D. Lee, O.S. Kwon, S.H. Song, Tailoring the performance of magnetic elastomers containing Fe2O3 decorated carbon nanofiber, RSC Adv. 7 (72) (2017) 45595–45600.

[7] Y.H. Wang, X.R. Zhang, K.H. Chung, C.C. Liu, S.B. Choi, H.J. Choi, Formation of core-shell structured complex microparticles during fabrication of magnetorheological elastomers and their magnetorheological behavior, Smart Mater. Struct. 25 (11) (2016) 115028.

[8] A.K. Bastola, V.T. Hoang, L. Li, A novel hybrid magnetorheological elastomer developed by 3D printing, Mater. Des. 114 (2017) 391–397.

[9] H.M. Pang, S.H. Xuan, T.X. Liu, X.L. Gong, Magnetic field dependent electroconductivity of the graphite doped magnetorheological plastomers, Soft Matter 11 (34) (2015) 6893–6902.

[10] I. Bica, E.M. Anitas, M. Bunoiu, B. Vatzulik, I. Juganaru, Hybrid magnetorheological elastomer: influence of magnetic field and compression pressure on its electrical conductivity, J. Ind. Eng. Chem. 20 (6) (2014) 3994–3999.

[11] Y. Shu, H. Tian, Y. Yang, C. Li, Y.L. Cui, W.T. Mi, Y.X. Li, Z. Wang, N.Q. Deng, B. Peng, T.L. Ren, Surface-modified piezoresistive nanocomposite flexible pressure sensors with high sensitivity and wide linearity, Nanoscale 7 (18) (2015) 8636–8644.

[12] T.D. Nguyen, H.S. Han, H.Y. Shin, C.T. Nguyen, H. Phung, H. Van Hoang, H.R. Choi, Highly sensitive flexible proximity tactile array sensor by using carbon micro coils, Sensors Actuators A 266 (2017) 166–177.

[13] S.F. Zhao, J.H. Li, D.X. Cao, G.P. Zhang, J. Li, K. Li, Y. Yang, W. Wang, Y.F. Jin, R. Sun, C.P. Wong, Recent advancements in flexible and stretchable electrodes for electromechanical sensors: strategies, materials, and features, ACS Appl. Mater. Interfaces 9 (14) (2017) 12147–12164.

[14] Y.S. Rim, S.H. Bae, H.J. Chen, N. De Marco, Y. Yang, Recent progress in materials and devices toward printable and flexible sensors, Adv. Mater. 28 (22) (2016) 4415–4440.

[15] T.Q. Trung, N.E. Lee, Flexible and stretchable physical sensor integrated platforms for wearable human-activity monitoring and personal healthcare, Adv. Mater. 28 (22) (2016) 4338–4372.

[16] W. Zhao, T. Rovere, D. Weerawarne, G. Osterhoudt, N. Kang, P. Joseph, J. Luo, B. Shim, M. Poliks, C.J. Zhong, Nanoalloy printed and pulse-laser sintered flexible sensor devices with enhanced stability and materials compatibility, ACS Nano 9 (6) (2015) 6168–6177.

[17] T.T. Tung, C. Robert, M. Castro, J.F. Feller, T.Y. Kim, K.S. Suh, Enhancing the sensitivity of graphene/polyurethane nanocomposite flexible piezo-resistive pressure sensors with magnetite nano-spacers, Carbon 108 (2016) 450–460.

[18] D.Y. Wang, L.Q. Tao, Y. Liu, T.Y. Zhang, Y. Pang, Q. Wang, S. Jiang, Y. Yang, T.L. Ren, High performance flexible strain sensor based on self-locked overlapping graphene sheets, Nanoscale 8 (48) (2016) 20090–20095.

[19] K.H. Kim, S.K. Hong, N.S. Jang, S.H. Ha, H.W. Lee, J.M. Kim, Wearable resistive pressure sensor based on highly flexible carbon composite conductors with irregular surface morphology, ACS Appl. Mater. Interfaces 9 (20) (2017) 17500–17508.

[20] A. Zuruzi, T.M. Haffiz, D. Affidah, A. Amirul, A. Norfatriah, M.H. Nurmawati, Towards wearable pressure sensors using multiwall carbon nanotube/polydimethylsiloxane nanocomposite foams, Mater. Des. 132 (2017) 449–458.

[21] L.H. Wang, L.H. Cheng, Piezoresistive effect of a carbon nanotube silicone-matrix composite, Carbon 71 (2014) 319–331.

[22] H.J. Kim, Y.J. Kim, High performance flexible piezoelectric pressure sensor based on CNT-sdoped 0-3 ceramic-epoxy nanocomposites, Mater. Des. 151 (2018) 133–140.

[23] Z. Chen, T. Ming, M.M. Goulamaly, H.M. Yao, D. Nezich, M. Hempel, M. Hofmann, J. Kong, Enhancing the sensitivity of percolative graphene films for flexible and transparent pressure sensor arrays, Adv. Funct. Mater. 26 (28) (2016) 5061–5067.

[24] Y.J. Zhu, J. Moran-Mirabal, Highly bendable and stretchable electrodes based on micro/nanostructured gold films for flexible sensors and electronics, Adv. Electron. Mater. 2 (3) (2016) 1500345.

[25] R. Mangayil, S. Rajala, A. Pammo, E. Sarlin, J. Luo, V. Santala, M. Karp, S. Tuukkanen, Engineering and characterization of bacterial nanocellulose films as low cost and flexible sensor material, ACS Appl. Mater. Interfaces 9 (22) (2017) 19048–19056.

[26] B.B. Nie, X.M. Li, J.Y. Shao, X. Li, H.M. Tian, D.R. Wang, Q. Zhang, B.H. Lu, Flexible and transparent strain sensors with embedded multiwalled carbon nanotubes meshes, ACS Appl. Mater. Interfaces 9 (46) (2017) 40681–40689.

[27] J. DeGraff, R. Liang, M.Q. Le, J.F. Capsal, F. Ganet, P.J. Cottinet, Printable low-cost and flexible carbon nanotube buckypaper motion sensors, Mater. Des. 133 (2017) 47–53.

[28] Y.Y. Qin, Q.Y. Peng, Y.J. Ding, Z.S. Lin, C.H. Wang, Y. Li, J.J. Li, Y. Yuan, X.D. He, Y.B. Li, Lightweight, superelastic, and mechanically flexible graphene/polyimide nanocomposite foam for strain sensor application, ACS Nano 9 (9) (2015) 8933–8941.

[29] X.X. Yin, T.P. Vinoda, R. Jelinek, A flexible high-sensitivity piezoresistive sensor comprising a Au nanoribbon-coated polymer sponge, J. Mater. Chem. C 3 (35) (2015) 9247–9252.

[30] A. Rinaldi, A. Tamburrano, M. Fortunato, M.S. Sarto, A flexible and highly sensitive pressure sensor based on a PDMS foam coated with graphene nanoplatelets, Sensors 16 (12) (2016) 2148.

[31] W.J. Huang, K. Dai, Y. Zhai, H. Liu, P.F. Zhan, J.C. Gao, G.Q. Zheng, C.T. Liu, C.Y. Shen, Flexible and lightweight pressure sensor based on carbon nanotube/thermoplastic polyurethane-aligned conductive foam with superior compressibility and stability, ACS Appl. Mater. Interfaces 9 (48) (2017) 42266–42277.

[32] Y.W. Liu, H.J. Zheng, M.X. Liu, High performance strain sensors based on chitosan/carbon black composite sponges, Mater. Des. 141 (2018) 276–285.

[33] X.C. Dong, Y. Wei, S. Chen, Y. Lin, L. Liu, J. Li, A linear and large-range pressure sensor based on a graphene/silver nanowires nanobiocomposites network and a hierarchical structural sponge, Compos. Sci. Technol. 155 (2018) 108–116.

[34] H.B. Yao, J. Ge, C.F. Wang, X. Wang, W. Hu, Z.J. Zheng, Y. Ni, H. Yu, A flexible and highly pressure-sensitive graphene-polyurethane sponge based on fractured microstructure design, Adv. Mater. 25 (46) (2013) 6692–6698.

[35] Y.S. Jun, S. Sy, W. Ahn, H. Zarrin, L. Rasen, R. Tjandra, B.M. Amoli, B.X. Zhao, G. Chiu, A.P. Yu, Highly conductive interconnected graphene foam based polymer composite, Carbon 95 (2015) 653–658.

[36] L. Ge, X.L. Gong, Y. Wang, S.H. Xuan, The conductive three dimensional topological structure enhanced magnetorheological elastomer towards a strain sensor, Compos. Sci. Technol. 135 (2016) 92–99.

[37] S. Yun, X.F. Niu, Z.B. Yu, W.L. Hu, P. Brochu, Q.B. Pei, Compliant silver nanowire-polymer composite electrodes for bistable large strain actuation, Adv. Mater. 24 (10) (2012) 1321–1327.

[38] W.L. Hu, X.F. Niu, R. Zhao, Q.B. Pei, Elastomeric transparent capacitive sensors based on an interpenetrating composite of silver nanowires and polyurethane, Appl. Phys. Lett. 102 (8) (2013), 083303.

[39] Y. Cheng, R.R. Wang, H.T. Zhai, J. Sun, Stretchable electronic skin based on silver nanowire composite fiber electrodes for sensing pressure, proximity, and multidirectional strain, Nanoscale 9 (11) (2017) 3834–3842.

[40] Z.Q. Wei, Z.K. Zhou, Q.Y. Li, J.C. Xue, A. Di Falco, Z.J. Yang, J.H. Zhou, X.H. Wang, Flexible nanowire cluster as a wearable colorimetric humidity sensor, Small 13 (27) (2017) 1700109.

[41] J.W. Kremenak, C.J. Arendse, F.R. Cummings, Y.Y. Chen, P.F. Miceli, Insight on the silver catalyst distribution during silicon nanowire array formation: an X-ray reflectivity study, Nanoscale 9 (48) (2017) 19073–19085.

[42] J.H. Seo, I. Hwang, H.D. Um, S. Lee, K. Lee, J. Park, H. Shin, T.H. Kwon, S.J. Kang, K. Seo, Cold isostatic-pressured silver nanowire electrodes for flexible organic solar cells via room-temperature processes, Adv. Mater. 29 (30) (2017).

[43] T. Joshi, J.H. Kang, L.L. Jiang, S. Wang, T. Tarigo, T.R. Lyu, S. Kahn, Z.W. Shi, Y.R. Shen, M.F. Crommie, F. Wang, Coupled one-dimensional plasmons and two-dimensional phonon polaritons in hybrid silver nanowire/silicon carbide structures, Nano Lett. 17 (6) (2017) 3662–3667.

[44] M. Amjadi, A. Pichitpajongkit, S. Lee, S. Ryu, I. Park, Highly stretchable and sensitive strain sensor based on silver nanowire-elastomer nanocomposite, ACS Nano 8 (5) (2014) 5154–5163.

[45] J. Ge, H.B. Yao, X. Wang, Y.D. Ye, J.L. Wang, Z.Y. Wu, J.W. Liu, F.J. Fan, H.L. Gao, C.L. Zhang, S.H. Yu, Stretchable conductors based on silver nanowires: improved performance through a binary network design, Angew. Chem. Int. Ed. 52 (6) (2013) 1654–1659.